



A facile preparation of WS₂ nanosheets as a highly effective HER catalyst

Xiangyong Zhang¹ · Hao Fei¹ · Zhuangzhi Wu^{1,2} · Dezhi Wang^{1,2}

Received: 1 February 2019 / Revised: 7 March 2019 / Accepted: 11 March 2019 / Published online: 24 April 2019
© The Nonferrous Metals Society of China 2019

Abstract

Tungsten disulfide (WS₂) has been considered as a promising hydrogen evolution reaction (HER) candidate due to its high activity, robust chemical stability, and earth-abundant resources. However, the inert basal planes and low electrical conductivity greatly hinder its development in HER. Increasingly, the density of active sites through the structural designing is one of the most effective strategies to enhance the HER performance. Herein, we report a facile one-step hydrothermal method for synthesizing flower-like WS₂ nanosheets for highly efficient HER. Besides, the effect of preparation temperature is also been discussed. The optimized WS₂ nanosheets exhibit the enhanced HER activity in strong acidic solutions with a low Tafel slope and a good stability. The improvement of the HER performance can be attributed to sheet-like nanostructures, which greatly increase the edge sites and defects, resulting in a high density of exposed active sites. Besides, these sheet-like nanostructures also can make the acidic electrolyte easily accessible to the surface of WS₂ and accelerate the electron transfer rate.

Keywords Tungsten disulfide · Nanosheet · Electrocatalyst · Hydrogen evolution reaction · Hydrothermal method

1 Introduction

Exploring renewable carbon-free energy alternatives is one of the most promising pathways for alleviating the energy and environmental crisis [1, 2]. Hydrogen has been considered as one of the most promising clean energy carriers because of its high energy density and no pollutant product [3]. Moreover, electrochemical water splitting is a highly efficient sustainable hydrogen production route [4]. However, the corresponding hydrogen production process always requires excellent catalysts to achieve fast kinetics and lower the overpotential for HER. Up to now, although platinum (Pt) and other Pt-group metals exhibit the best catalytic activity for HER, the scarcity and high cost impede their widespread applications [5]. Thus, there is still an urgent

demand for developing earth-abundant catalysts to replace these noble metal catalysts for effective HER.

Recently, a large variety of non-precious metal candidates, including transition metal carbides [6–9], phosphides [10–13], chalcogenides [14–20] and so on, have been investigated and shown striking HER performances. Among these alternatives, tungsten disulfide (WS₂) has received persistent interest for its high activity, robust chemical stability, and earth-abundant resources [21]. However, both theoretical and experimental studies revealed that the edge state possesses a lower hydrogen adsorption Gibbs free energy, which means that HER performance mainly arises from the edge site, while the large-area basal planes are catalytically inert and useless for HER [22–24]. Moreover, as a semiconductor material, the activity of WS₂ is primarily limited by its low electrical conductivity, which restricts charge transfer kinetics for HER [25]. Considering the above two factors, there are generally two routes to enhance the catalytic activity of WS₂. One is to increase the density of the exposed active sites. Among large amounts of methods, structural designing is one of the most effective strategies for increasing the number of active sites [26, 27]. In our previous work [28], the WS₂ nanosheets (NSs) with loosely stacked layers were successfully obtained by a mechanical activation strategy. This special nanostructure provides highly exposed rims and

✉ Zhuangzhi Wu
zwu2012@csu.edu.cn

✉ Dezhi Wang
dzwang@csu.edu.cn

¹ School of Materials Science and Engineering, Central South University, Changsha 410083, China

² Key Laboratory of Ministry of Education for Non-ferrous Materials Science and Engineering, Changsha 410083, China

edges for HER. Cheng et al. [29] synthesized the ultrathin WS₂ nanoflakes by the high-temperature solution-phase method. The obtained catalyst possessed abundant edges and the ultrathin thickness. By directly vulcanizing the WO₃ nanosheets, Shang et al. [30] fabricated a WS₂/WO₃ heterostructure which could expose abundant active sites for HER. The other route is to improve the electrical conductivity. Sun et al. [31] synthesized the N-doped WS₂ nanosheets by one-step sol-gel process and found that N doping in WS₂ might be an effective way to improve the intrinsic conductivity of WS₂. Duan et al. [32] fabricated 3D WS₂ nanolayers@heteroatom-doped graphene films via a vacuum-filtration process, and the conductive network of graphene sheets greatly accelerates the charge transfer kinetics. Despite these developments, the HER activity of WS₂ is still much lower than that of Pt. Thus, it is still a big challenge to further improve the HER performance of WS₂.

Herein, the flower-like WS₂ nanosheets were synthesized via a facile one-pot hydrothermal method. This unique nanostructure not only can greatly increase the edge sites and defects, resulting in a high density of exposed active sites, but also can make the acidic electrolyte easily accessible to the surface of WS₂ and accelerate the electron transfer rate. Moreover, the HER performance of WS₂ is improved by controlling the reaction temperature. As a result, the optimized WS₂ NSs exhibit a good HER activity in an acidic solution with a small Tafel slope of 70 mV dec⁻¹ and a good stability.

2 Experimental

2.1 Materials

Sodium tungstate dihydrate (Na₂WO₄·2H₂O), sodium hypophosphite (NaH₂PO₂·H₂O), thioacetamide (CH₃CSNH₂) and bulk WS₂ were purchased from Aladdin. The Pt/C catalyst (20 wt.%) was purchased from the Johnson Matthey and Nafion solution (5 wt.%) was purchased from the DuPont.

2.2 Synthesis of WS₂

Typically, 0.99 g Na₂WO₄·2H₂O, 0.32 g NaH₂PO₂·H₂O and 1.13 g CH₃CSNH₂ were dissolved into 50 mL distilled water. After being stirred to form a transparent solution, 0.75 mL concentrated HCl was dropped into the solution and continuously stirred for 30 min. Then, the solution was transferred into a 100 mL Teflon-lined stainless-steel autoclave, and heated in an oven maintained at 180–220 °C for 24 h. After being naturally cooled to room temperature, the as-prepared samples were obtained by centrifugation, washed

by absolute ethanol and deionized water for several times, and dried at 80 °C overnight.

2.3 Preparation of working electrodes

In a typical procedure, 3 mg of the catalyst was added into the solution containing 80 μL Nafion solution (5 wt.%), 0.2 mL absolute ethanol and 0.8 mL deionized water. After being sonicated for 30 min, 5 mL of the formed homogeneous slurry was dropped onto a smooth glassy carbon electrode (GCE) of 3 mm in diameter, generating a working electrode with a loading of 213 μg cm⁻².

2.4 Physical measurements

The powder XRD patterns were recorded using the Mini Flex 600 system, and the Raman spectroscopy was obtained on the LabRAMHR-800 (French company HRIBA). The transmission electron microscopy (TEM) images and the scanning electron microscopy (SEM) images were acquired on the Tecnai G² F20 and the FEI Sirion 200, respectively. The X-ray photoelectron spectroscopy (XPS) was conducted on the ESCALAB 250Xi and the correspond binding energy values were corrected via the C1s.

2.5 Electrochemical measurements

A CHI660E workstation (CH Instruments, China) with a standard three-electrode system was used to perform all the electrochemical tests. The modified GCE was used as the working electrode, and the carbon rod and the saturated Hg/Hg₂Cl₂ electrode (SCE) were served as the counter electrode and the reference electrode, respectively. The linear sweep voltammetry (LSV) was carried out in 0.5 mol L⁻¹ H₂SO₄ using a sweep rate of 2 mV s⁻¹ from 0.1 to -0.4 V (vs. SCE). The long-term cycling test was performed via the cyclic voltammetry (CV) measurements with a sweep rate of 50 mV s⁻¹ from 0.1 to -0.4 V for 2000 cycles. In addition, the electrochemical impedance spectroscopy (EIS) was conducted between the frequency range of 10⁶ Hz and 1 Hz with a sinusoidal perturbation of 5 mV at an overpotential of -300 mV.

2.6 Electrochemical measurements

The electrochemically capacitance measurements were conducted by cyclic voltammograms from 0.00 to 0.20 V with various scan rates (20, 40, 60, 80, 100, 120, 140 mV s⁻¹). The capacitive currents were measured in a potential where no faradic processes were observed, i.e., at 0.1 V versus RHE. According to the previous report [14], the specific capacitance, a flat standard with 1 cm² of the real surface

area, is approximately $60 \mu\text{F cm}^{-2}$. Thus, the electrochemical active surface area can be calculated by the following Eq. (1):

$$A_{\text{ECSA}} = \frac{\text{electrochemical capacitance}}{60 \mu\text{F cm}^{-2} (\text{per cm}^2_{\text{ECSA}})} \quad (1)$$

3 Results and discussion

3.1 Microstructural characterization

The XRD pattern of WS₂ NSs is shown in Fig. 1a. The peaks at 14.2° , 32.1° , 35.4° , 43.4° and 56.9° can be assigned to the (002), (100), (102), (006), and (110) planes of WS₂ (JCPDS No. 08-0237), respectively. There are no major impurities detected, suggesting the high purity of the obtained WS₂. Besides, the XRD pattern of bulk WS₂ is also given for a comparison, which is well consistent with the standard WS₂. Interestingly, compared with the bulk WS₂, all peaks of WS₂ NSs are weaker and broader, indicating a poor crystallinity and disordered structure [33]. Raman spectroscopy was conducted to further confirm the structure of WS₂ NSs. As shown in Fig. 1b, there are two pronounced peaks at ~ 50 and 420 cm^{-1} , which are assignable to the E_{2g}^1 modes and the A_{1g} modes of 2H-WS₂, respectively [34, 35]. Compared with the bulk WS₂, the Raman peaks of WS₂ NSs show slight shifts, which can be attributed to the possible changes in the bond polarization [36].

The morphologies of as-prepared WS₂ and bulk WS₂ are shown in Fig. 2. It can be seen from Fig. 2a, d that the as-prepared WS₂ exhibits a flower-like morphology, which is consisted of a large number of loosely assembled thin nanosheets. The high-resolution TEM (HRTEM) image (Fig. 2e) of the WS₂ NSs reveals that the interlayer spacing of the WS₂ (002) planes is $\sim 0.62 \text{ nm}$. In Fig. 2b, the

pristine bulk WS₂ shows large and thick bulk morphology. The HRTEM image (Fig. 2c) suggests that the basal plane of the bulk WS₂ possesses high crystallinity and no defects. As for the basal plane of WS₂ NSs (Fig. 2f), many defects (the yellow selection in Fig. 2f) can be observed, which may be beneficial for HER as possible active sites.

To get insights into the surface chemical valence states of WS₂ NSs, the XPS analysis was further performed (Fig. 3). As shown in Fig. 3a, the high-resolution W 4f spectra can be fitted into two doublets. The doublets located at binding energies of 38.2 eV (W 4f_{5/2}) and 36.1 eV (W 4f_{7/2}) are originated from W⁶⁺ in WO₃, which can be ascribed to surface oxidation of WS₂ [25, 30, 37]. The peaks located at 34.4 eV and 32.3 eV are assigned to 4f_{5/2} and 4f_{7/2} of W⁴⁺, respectively, which are consistent with the presence of WS₂ [38, 39]. Correspondingly, the doublets at around 163.0 eV and 161.8 eV (Fig. 3b) are indexed to 2p_{3/2} and 2p_{1/2} of S, respectively, which can be attributed to S²⁻ species in WS₂ [40, 41].

3.2 Insights into the HER kinetics

The electrochemical performance of the bulk WS₂ and WS₂ NSs for HER was detected by the LSV measurement in $0.5 \text{ mol L}^{-1} \text{ H}_2\text{SO}_4$. The polarization curves of different catalysts are shown in Fig. 4a, and the key electrochemical results are also displayed in Table 1. The commercial Pt/C catalyst (20 wt.%, Johnson Matthey) was also measured as a reference. The bulk WS₂ exhibits a poor HER performance with a high onset potential (the current density reaches 1 mA cm^{-2}) of -396 mV , and low current density (j_{-400}) of 1.1 mA cm^{-2} at a specific overpotential of -400 mV . In comparison, the WS₂ NSs exhibits a good HER activity with a low onset potential of -306 mV , and a high j_{-400}

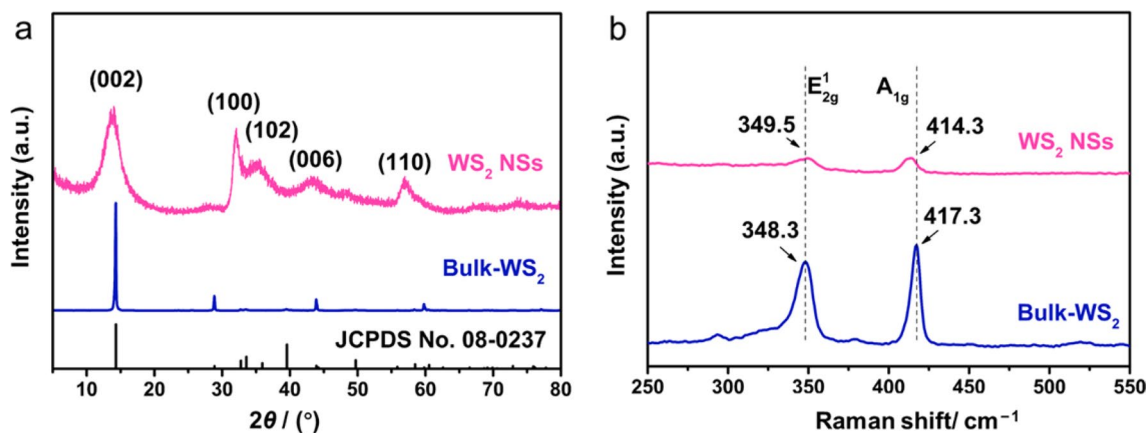


Fig. 1 a XRD patterns and b Raman spectra of the WS₂ NSs and bulk WS₂

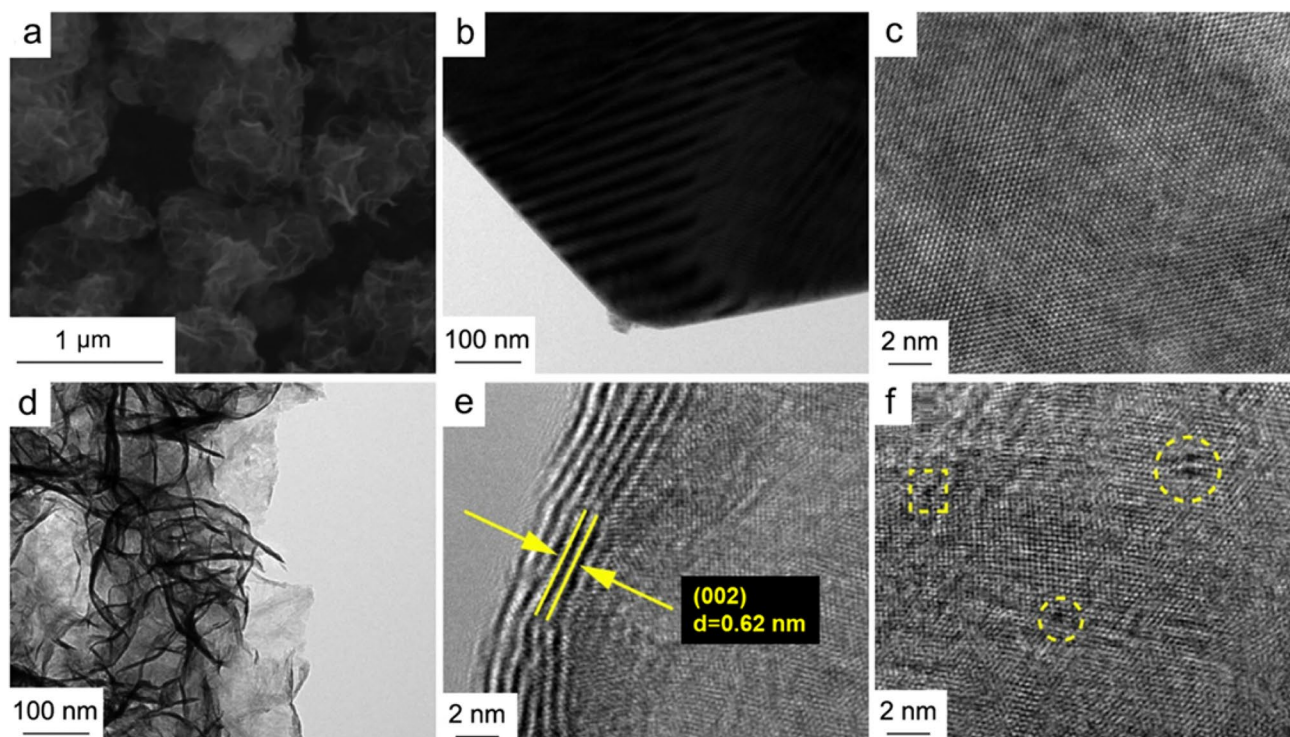


Fig. 2 **a** SEM image of WS₂ NSs; **b, c** TEM and HRTEM images of bulk WS₂; **d–f** TEM and HRTEM images of WS₂ NSs

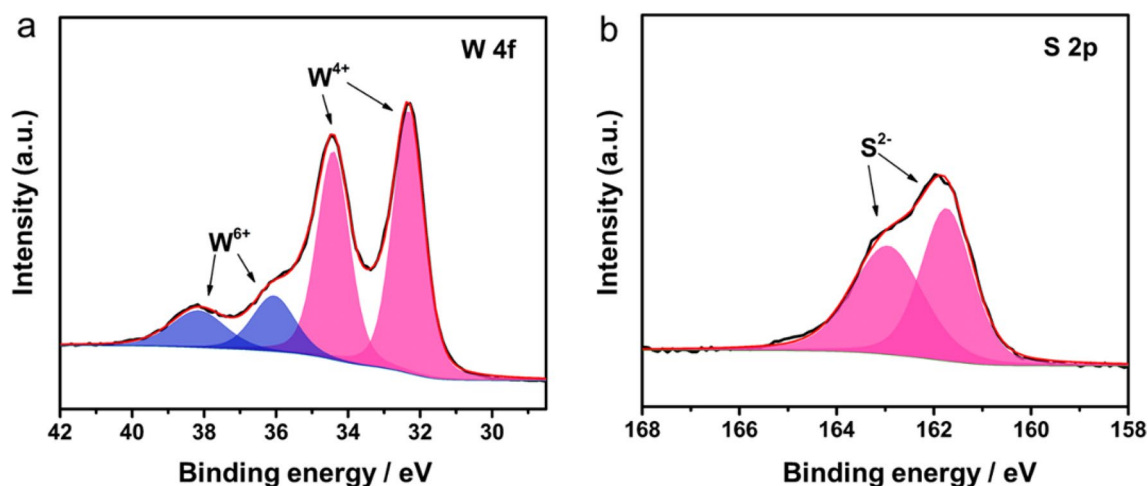


Fig. 3 XPS spectra of WS₂ NSs: **a** W 4f and **b** S 2p

of 8.5 mA cm⁻², which is ~7 times higher than that of the bulk WS₂.

To further study the catalytic activity of the WS₂ catalysts, the Tafel slopes were extracted from the corresponding LSV curves through the Tafel equation ($\eta = b \log j + a$, where a is the onset potential and b is the Tafel slope) (Fig. 4b). The WS₂ NSs exhibit a Tafel slope of 70 mV dec⁻¹, which is remarkably smaller than that of bulk WS₂ (112 mV dec⁻¹), indicating a more efficient HER process [42, 43]. Generally,

in acid media, it is accepted that the HER process involves two steps. The electrochemical adsorption of hydrogen (Volmer reaction, $H^+ + M + e^- \rightarrow M - H^*$, where M is the catalysts) is the first step. While, the desorption of adsorbed hydrogen is the second step, which includes the electrochemical desorption (Heyrovsky reaction, $M - H^* + H^+ + e^- \rightarrow M + H_2$) or the chemical desorption (Tafel reaction, $M - H^* + M - H^* \rightarrow 2M + H_2$). According to the classic theory, the Tafel slope can be used to evaluate

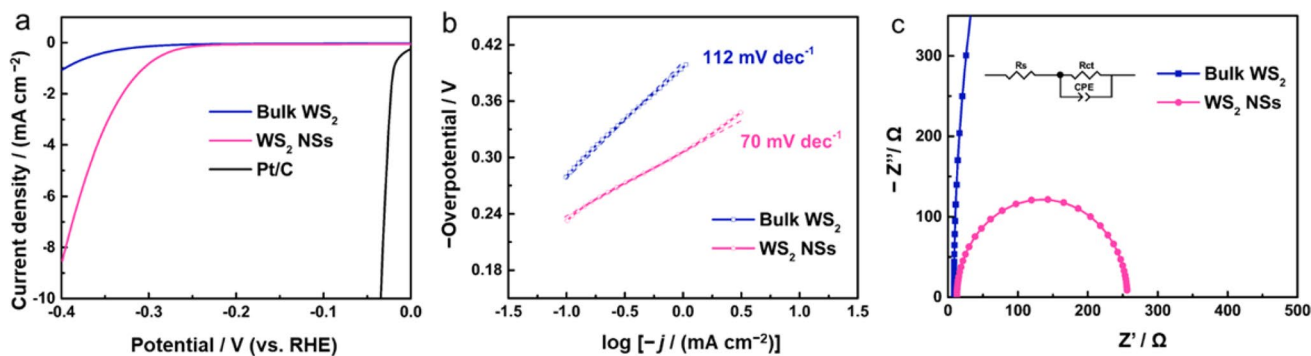


Fig. 4 **a** Polarization curves, **b** Tafel slopes and **c** Nyquist plots of the WS₂ NSs and the bulk WS₂; **d** Polarization curves of the WS₂ NSs and after 5000 cycles

Table 1 Summary of information over various WS₂ catalysts

Catalysts	Tafel slope / (mV dec ⁻¹)	η_1 / mV	j_{400} / (mA cm ⁻²)	C_{dl} / (mF cm ⁻²)	A_{ECSA} / cm ² _{ECSA}	R_{ct} / Ω
Bulk WS ₂	112	-396	1.1	0.2	3.33	5231
WS ₂ NSs	70	-306	8.5	11.4	190	244

ECSA electrochemically active surface area

the rate-determining step in the HER process [44–46]. Correspondingly, the Tafel slope values will reach 118, 29 and 39 mV dec⁻¹ if the Volmer, Tafel, and Heyrovsky reactions are the rate-determining steps, respectively. The small Tafel slope of 70 mV dec⁻¹ denotes that the WS₂ NSs undergo a mixed Volmer-Heyrovsky mechanism and the Heyrovsky reaction acts as the rate-determining step.

To get insights into electrode kinetics of the HER process, the EIS measurements were performed at a constant voltage of -300 mV. A simplified equivalent circuit (inserted in Fig. 4c) was utilized to fit the Nyquist plots. The charge transfer resistance (R_{ct}) can be determined from the semi-circle. The R_{ct} value of WS₂ NSs (244 Ω) is much smaller

than that of bulk WS₂ (5231 Ω), suggesting a faster electron transfer rate and superior kinetics of WS₂ NSs in HER process [47]. The small R_{ct} value of WS₂ NSs can be attributed the sheet-like nanostructure, which can make the acidic electrolyte easily accessible to the surface of WS₂, resulting in a faster electron transfer rate [48, 49]. On the contrary, the bulk structure of bulk WS₂ slows down the electron transfer rate, thus, leading to a large R_{ct} value.

Besides, the stability of catalysts is an important indicator for evaluating the electrocatalytic performance. The long-term cycling measurement of the WS₂ NSs was adopted using the CV. As shown in Fig. 5a, only a negligible shift of the current density can be observed after scanning for 2000

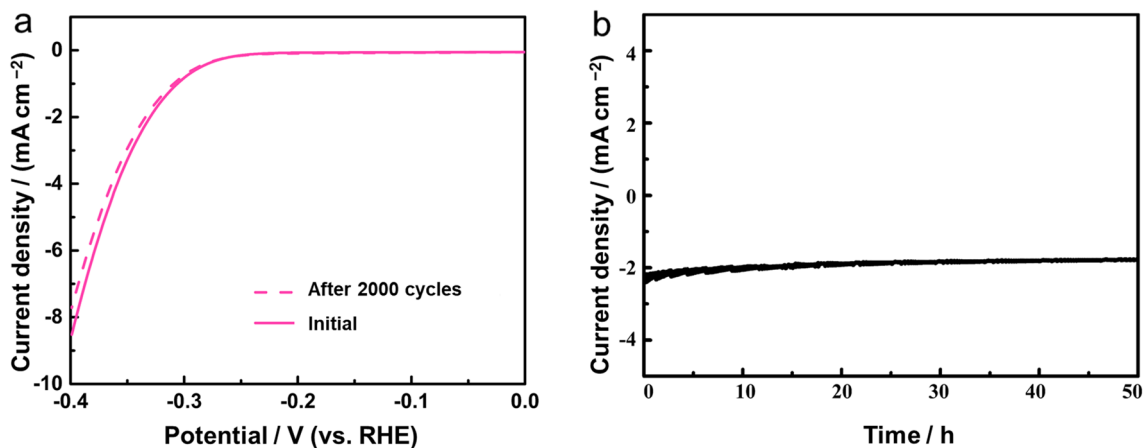


Fig. 5 **a** Polarization curves of the WS₂ NSs and after 2000 cycles; **b** $I-t$ curve of the WS₂ NSs for 50 h

cycles, implying the good catalytic stability of WS₂ NSs. The time-dependent current density curve ($I-t$ curve) was also obtained (Fig. 5b). Only a slight degradation of the current density over 50 h further proves its good stability. The SEM and TEM images of the WS₂ NSs after scanning for 2000 cycles are shown in Fig. 6, and there are few changes in the morphology after the stability test.

The ECSA of WS₂ catalysts was estimated by testing the double-layer capacitance (C_{dl}) at non-faradaic potentials (Fig. 7). A higher ECSA value means a larger density of active sites for WS₂. Figure 7c is the measured current density plotted as a function of the scan rate, in which the C_{dl} value is equivalent to the slope value. A direct comparison of these two samples can be obtained because the ECSA value is proportional to the C_{dl} value. One can see that the C_{dl} value of the WS₂ NSs is 11.2 mF cm⁻², whereas the C_{dl} value of the bulk WS₂ is 0.2 mF cm⁻². Accordingly, the WS₂ NSs exhibits a high ECSA value of 190 cm²_{ECSA} ~ 57 times as high as that of the bulk WS₂ (3.33 cm²_{ECSA}), suggesting that the WS₂ NSs possess plenty of edge sites and defects that will greatly increase the density of active sites.

Due to the hydrothermal reaction being sensitive to the preparation temperature, the effect of the preparation

temperature is also been discussed. All the as-prepared WS₂ NSs are named as WS₂-XXX for convenience, where XXX represents the preparation temperature in the unit of °C. In Fig. 8a, one can see that the HER activity of WS₂ NSs firstly increases with the increase of the preparation temperature and reaches the maximum at 200 °C, and then decreases at higher temperatures, which means that 200 °C is the most suitable temperature for the formation of the high-efficiency HER catalyst in WS₂ NSs. Similar regulations can also be found in Tafel and Nyquist plots (Fig. 8b, c). In general, as the preparation temperature increases, the crystallinity of the as-prepared catalysts is improved, leading to a decrease in the number of defects and a corresponding decrease in the number of active sites. While, on the other hand, a higher crystallinity of the WS₂ NSs could result in a better conductivity [50]. Thus, we believe that a balance is achieved between the number of active sites and conductivity at 200 °C, resulting in the best HER performance.

As a result, the good HER activity of the optimized WS₂-200 can be ascribed to a sheet-like structure, which not only can greatly increase the number of exposed active sites, but also can make the acidic electrolyte easily accessible to the surface of WS₂ and accelerate the electron transfer rate.

Fig. 6 **a** SEM image and **b** TEM image of WS₂ NSs after scanning for 2000 cycles

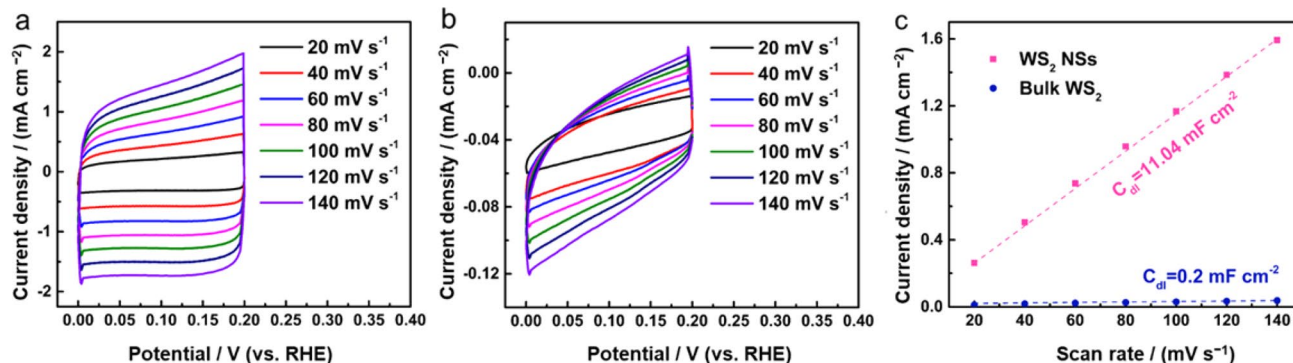
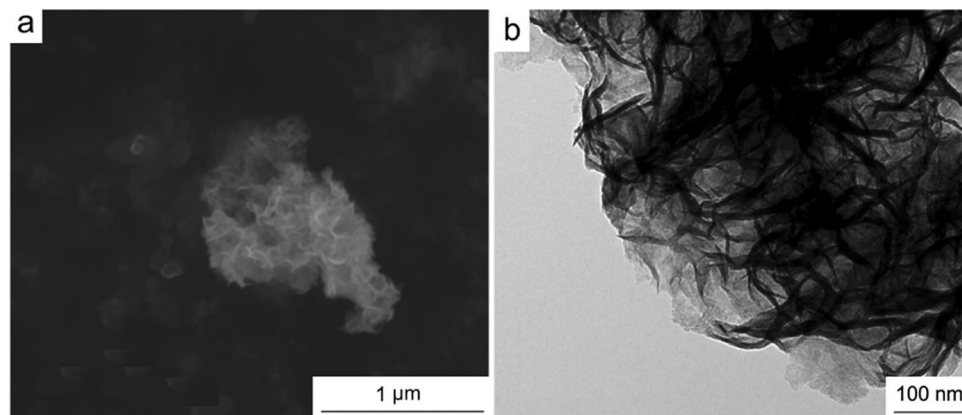


Fig. 7 Electrochemical capacitance measurements: **a** WS₂ NSs and **b** bulk WS₂; **c** Measured capacitive current densities (at 100 mV vs. RHE) plotted as a function of the scan rate for the WS₂ NSs and bulk WS₂

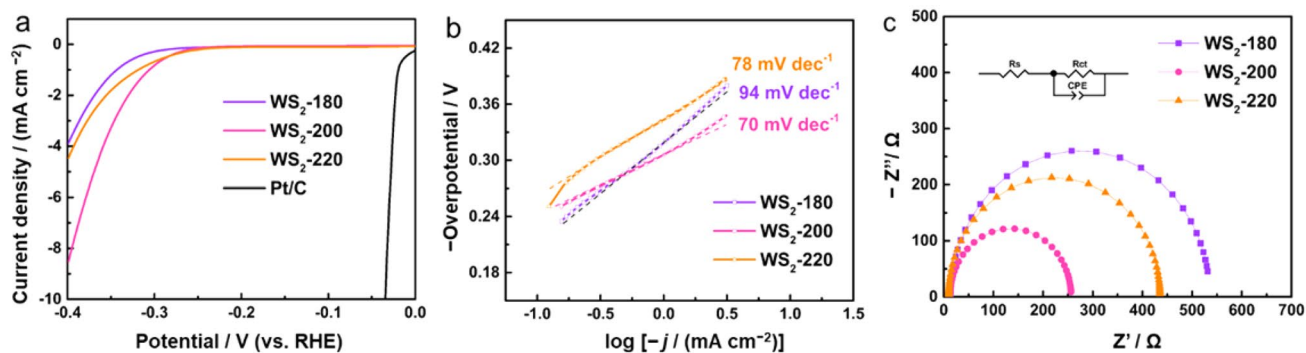


Fig. 8 a Polarization curves, b Tafel slopes and c Nyquist plots of the WS₂ NSs obtained at various temperatures

Besides, the appropriate preparation temperature is also important, which makes the WS₂-200 possess a relatively large number of active sites and high conductivity, in the same time.

4 Conclusion

In summary, a flower-like WS₂ catalyst is successfully synthesized via a facile one-pot hydrothermal method. The unique nanostructure can greatly increase the edge sites and defects, resulting in a high density of exposed active sites. Compared with bulk WS₂, the WS₂ NSs show a high ECSA value of 190 cm²_{ECSA}, ~7 times as high as that of bulk WS₂; and a high j_{-400} of 8.5 mA cm⁻², ~7 times higher than bulk WS₂ and a lower Tafel slope of 70 mV dec⁻¹. Moreover, the good stability also makes it a promising alternative to replace precious-metal HER catalysts. Besides, the effect of preparation temperature is also discussed, and 200 °C is found to be the best preparation temperature for WS₂ NSs.

Acknowledgements Financial supports from the National Natural Science Foundation of China (Grant 51572301), National Key R&D Program of China (2017YFB0306001 and 2018YFC1901702), Hunan Provincial Natural Science Foundation (Grant 2016JJ3153) and the Innovation-Driven Project of Central South University (Grant 502221802) are gratefully acknowledged.

References

- Dresselhaus MS, Thomas IL. Alternative energy technologies. *Nature*. 2001;414:332.
- Turner JA. Sustainable hydrogen production. *Science*. 2004;305(5686):972.
- Tang CY, Wang W, Sun AK, Qi C, Zhang DZ, Wu ZZ, Wang DZ. Sulfur-decorated molybdenum carbide catalysts for enhanced hydrogen evolution. *ACS Catal*. 2015;5(11):6956.
- Wang DZ, Zhang XY, Bao SY, Zhang ZT, Fei H, Wu ZZ. Phase engineering of a multiphase 1T/2H MoS₂ catalyst for highly efficient hydrogen evolution. *J Mater Chem A*. 2017;5(6):2681.
- Huang XL, Leng M, Xiao W, Li M, Ding J, Tan TL, Lee WSV, Xue JM. Activating basal planes and S-Terminated edges of MoS₂ toward more efficient hydrogen evolution. *Adv Funct Mater*. 2017;27(6):1604943.
- Tang CY, Sun AK, Xu YS, Wu ZZ, Wang DZ. High specific surface area Mo₂C nanoparticles as an efficient electrocatalyst for hydrogen evolution. *J Power Sources*. 2015;296:18.
- Fan XJ, Liu YY, Peng ZW, Zhang ZH, Zhou HQ, Zhang XM, Yakobson BI, Goddard WA, Guo X, Hauge RH, Tour JM. Atomic H-Induced Mo₂C hybrid as an active and stable bifunctional electrocatalyst. *ACS Nano*. 2017;11(1):384.
- Wang DZ, Guo T, Wu ZZ. Hierarchical Mo₂C/C scaffolds organized by nanosheets as highly efficient electrocatalysts for hydrogen production. *ACS Sustain Chem Eng*. 2018;6(11):13995.
- Wang DZ, Liu TY, Wang JC, Wu ZZ. N, P (S) Co-doped Mo₂C/C hybrid electrocatalysts for improved hydrogen generation. *Carbon*. 2018;139:845.
- Xiao P, Sk MA, Thia L, Ge XM, Lim RJ, Wang JY, Lim KH, Wang X. Molybdenum phosphide as an efficient electrocatalyst for the hydrogen evolution reaction. *Energy Environ Sci*. 2014;7(8):2624.
- Zhang XY, Wu ZZ, Wang DZ. Oxygen-incorporated defect-rich MoP for highly efficient hydrogen production in both acidic and alkaline media. *Electrochim Acta*. 2018;281:540.
- Wang DZ, Zhang XY, Zhang DZ, Shen YL, Wu ZZ. Influence of Mo/P ratio on CoMoP nanoparticles as highly efficient HER catalysts. *Appl Catal A Gen*. 2016;511:11.
- Chen XB, Wang DZ, Wang ZP, Zhou P, Wu ZZ, Jiang F. Molybdenum phosphide: a new highly efficient catalyst for the electrochemical hydrogen evolution reaction. *Chem Commun*. 2014;50(79):11683.
- Lukowski MA, Daniel AS, English CR, Meng F, Forticaux A, Hamers RJ, Jin S. Highly active hydrogen evolution catalysis from metallic WS₂ nanosheets. *Energy Environ Sci*. 2014;7(8):2608.
- Wu ZZ, Tang CY, Zhou P, Liu ZH, Xu YS, Wang D, Fang B. Enhanced hydrogen evolution catalysis from osmotically swollen ammoniated MoS₂. *J Mater Chem A*. 2015;3(24):13050.
- Wang DZ, Zhang XY, Shen YL, Wu ZZ. Ni-doped MoS₂ nanoparticles as highly active hydrogen evolution electrocatalysts. *RSC Adv*. 2016;6(20):16656.
- Shi Y, Zhou Y, Yang DR, Xu WX, Wang C, Wang FB, Xu JJ, Xia XH, Chen HY. Energy level engineering of MoS₂ by transition-metal doping for accelerating hydrogen evolution reaction. *J Am Chem Soc*. 2017;139(43):15479.
- Wang LL, Zhang QF, Zhu JY, Duan XD, Xu Z, Liu YT, Yang HG, Lu BG. Nature of extra capacity in MoS₂ electrodes: molybdenum atoms accommodate with lithium. *Energy Storage Mater*. 2019;16:37.

19. Li Y, Yin K, Wang LL, Lu XL, Zhang YQ, Liu YT, Yan DF, Song YZ, Luo SL. Engineering MoS₂ nanomesh with holes and lattice defects for highly active hydrogen evolution reaction. *Appl Catal B*. 2018;239:537.
20. Liu CB, Wang LL, Tang YH, Luo SL, Liu YT, Zhang SQ, Zeng YX, Xu YZ. Vertical single or few-layer MoS₂ nanosheets rooting into TiO₂ nanofibers for highly efficient photocatalytic hydrogen evolution. *Appl Catal B*. 2015;164:1.
21. He QY, Wang LL, Yin K, Luo SL. Vertically aligned ultrathin 1T-WS₂ nanosheets enhanced the electrocatalytic hydrogen evolution. *Nanoscale Res Lett*. 2018;13(1):167.
22. Karunadasa HI, Montalvo E, Sun YJ, Majda M, Long JR, Chang CJ. A Molecular MoS₂ edge site mimic for catalytic hydrogen generation. *Science*. 2012;335(6069):698.
23. Ramakrishna Matte HSS, Gomathi A, Manna AK, Late DJ, Datta R, Pati SK, Rao CNR. MoS₂ and WS₂ Analogues of Graphene. *Angew Chem Int Edit*. 2010;49(24):4059.
24. Babu G, Masurkar N, Al Salem H, Arava LMR. Transition metal dichalcogenide atomic layers for lithium polysulfides electrocatalysis. *J Am Chem Soc*. 2017;139(1):171.
25. Shang X, Yan KL, Liu ZZ, Lu SS, Dong B, Chi JQ, Li X, Liu YR, Chai YM, Liu CG. Oxidized carbon fiber supported vertical WS₂ nanosheets arrays as efficient 3D nanostructure electrocatalysts for hydrogen evolution reaction. *Appl Surf Sci*. 2017;402:120.
26. Zhou G, Shan Y, Wang LL, Hu YY, Guo JH, Hu FR, Shen JC, Gu Y, Cui JT, Liu LZ, Wu XL. Photoinduced semiconductor-metal transition in ultrathin troilite FeS nanosheets to trigger efficient hydrogen evolution. *Nat Commun*. 2019;10(1):399.
27. Wang LL, Duan XD, Wang GM, Liu CB, Luo SL, Zhang SQ, Zeng YX, Xu YZ, Liu YT, Duan XF. Omnidirectional enhancement of photocatalytic hydrogen evolution over hierarchical "cauline leaf" nanoarchitectures. *Appl Catal B*. 2016;186:88.
28. Wu ZZ, Fang BZ, Bonakdarpour A, Sun AK, Wilkinson DP, Wang DZ. WS₂ nanosheets as a highly efficient electrocatalyst for hydrogen evolution reaction. *Appl Catal B*. 2012;125:59.
29. Cheng L, Huang WJ, Gong QF, Liu CH, Liu Z, Li YG, Dai HJ. Ultrathin WS₂ nanoflakes as a high-performance electrocatalyst for the hydrogen evolution reaction. *Angew Chem Int Edit*. 2014;53(30):7860.
30. Shang X, Rao Y, Lu SS, Dong B, Zhang LM, Liu XH, Li X, Liu YR, Chai YM, Liu CG. Novel WS₂/WO₃ heterostructured nanosheets as efficient electrocatalyst for hydrogen evolution reaction. *Mater Chem Phys*. 2017;197:123.
31. Sun CQ, Zhang JY, Ma J, Liu PT, Gao DQ, Tao K, Xue DS. N-doped WS₂ nanosheets: a high-performance electrocatalyst for the hydrogen evolution reaction. *J Mater Chem A*. 2016;4(29):11234.
32. Duan JJ, Chen S, Chambers BA, Andersson GG, Qiao SZ. 3D WS₂ nanolayers@heteroatom-doped graphene films as hydrogen evolution catalyst electrodes. *Adv Mater*. 2015;27(28):4234.
33. Xie JF, Wu CZ, Hu SL, Dai J, Zhang N, Feng J, Yang JL, Xie Y. Ambient rutile VO₂(R) hollow architectures with rich grain boundaries from new-state nsutite-type VO₂, displaying enhanced hydrogen adsorption behavior. *Phys Chem Chem Phys*. 2012;14(14):4810.
34. Krause M, Viršek M, Remškar M, Salacan N, Fleischer N, Chen LH, Hatto P, Kolitsch A, Möller W. Diameter and morphology dependent raman signatures of WS₂ nanostructures. *ChemPhysChem*. 2009;10(13):2221.
35. Berkdemir A, Gutiérrez HR, Botello-Méndez AR, Perea-López N, Elías AL, Chia CI, Wang B, Crespi VH, López-Urías F, Charlier JC, Terrones H, Terrones M. Identification of individual and few layers of WS₂ using raman spectroscopy. *Sci Rep*. 2013;3:1755.
36. Shifa TA, Wang FM, Liu KL, Cheng Z, Xu K, Wang ZX, Zhan XY, Jiang C, He J. Efficient catalysis of hydrogen evolution reaction from WS₂(1-x)P_{2x} nanoribbons. *Small*. 2017;13(16):1603706.
37. Liu ZQ, Li N, Su C, Zhao HY, Xu LL, Yin ZY, Li J, Du YP. Colloidal synthesis of 1T' phase dominated WS₂ towards durable electrocatalysis. *Nano Energy*. 2018;50:176.
38. Shang X, Chi JQ, Lu SS, Dong B, Li X, Liu YR, Yan KL, Gao WK, Chai YM, Liu CG. Novel Co_xS_y/WS₂ nanosheets supported on carbon cloth as efficient electrocatalyst for hydrogen evolution reaction. *Int J Hydrog Energy*. 2017;42(7):4165.
39. Hasani A, Nguyen TP, Tekalgne M, Van Le Q, Choi KS, Lee TH, Jung Park T, Jang HW, Kim SY. The role of metal dopants in WS₂ nanoflowers in enhancing the hydrogen evolution reaction. *Appl Catal A Gen*. 2018;567:73.
40. Zhang YX, Yan JQ, Ren XP, Pang LQ, Chen H, Liu SZ. 2D WS₂ nanosheet supported Pt nanoparticles for enhanced hydrogen evolution reaction. *Int J Hydrog Energy*. 2017;42(8):5472.
41. Yang L, Zhu XB, Xiong SJ, Wu XL, Shan Y, Chu PK. Synergistic WO₃·2H₂O nanoplates/WS₂ nanoplates/WS₂ hybrid catalysts for high-efficiency hydrogen evolution. *ACS Appl Mater Interfaces*. 2016;8(22):13966.
42. Zhang XY, Wang JC, Guo T, Liu TY, Wu ZZ, Cavallo L, Cao Z, Wang DZ. Structure and phase regulation in Mo_xC (α-MoC_{1-x}/β-Mo₂C) to enhance hydrogen evolution. *Appl Catal B*. 2019;247:78.
43. Yang YQ, Zhang WB, Xiao YL, Shi ZP, Cao XM, Tang Y, Gao QS. CoNiSe₂ heteronanorods decorated with layered-double-hydroxides for efficient hydrogen evolution. *Appl Catal B*. 2019;242:132.
44. Sudhagar P, Roy N, Vedarajan R, Devadoss A, Terashima C, Nakata K, Fujishima A. Hydrogen and CO₂ reduction reactions: mechanisms and catalysts. In: Giménez S, Bisquert J, editors. Photoelectrochemical solar fuel production: from basic principles to advanced devices. Cham: Springer international publishing; 2016. p. 105.
45. Li YG, Wang HL, Xie LM, Liang YY, Hong GS, Dai HJ. MoS₂ nanoparticles grown on graphene: an advanced catalyst for the hydrogen evolution reaction. *J Am Chem Soc*. 2011;133(19):7296.
46. Xie JF, Zhang H, Li S, Wang RX, Sun X, Zhou M, Zhou JF, Lou XW, Xie Y. Defect-rich MoS₂ ultrathin nanosheets with additional active edge sites for enhanced electrocatalytic hydrogen evolution. *Adv Mater*. 2013;25(40):5807.
47. Yin Y, Han JC, Zhang YM, Zhang XH, Xu P, Yuan Q, Samad L, Wang XJ, Wang Y, Zhang ZH, Zhang P, Cao XZ, Song B, Jin S. Contributions of phase, sulfur vacancies, and edges to the hydrogen evolution reaction catalytic activity of porous molybdenum disulfide nanosheets. *J Am Chem Soc*. 2016;138(25):7965.
48. Hu K, Zhou JH, Yi ZX, Ye CL, Dong HY, Yan K. Facile synthesis of mesoporous WS₂ for water oxidation. *Appl Surf Sci*. 2019;465:351.
49. Wang AQ, Li HB, Xiao JP, Lu YR, Zhang M, Hu K, Yan K. Integration of theory and experiment on mesoporous nickel sulfide microsphere for hydrogen evolution reaction. *ACS Sustain Chem Eng*. 2018;6(12):15995.
50. Wang DZ, Pan Z, Wu ZZ, Wang ZP, Liu ZH. Hydrothermal synthesis of MoS₂ nanoflowers as highly efficient hydrogen evolution reaction catalysts. *J Power Sources*. 2014;264:229.



Dr. Dezhi Wang born in 1968, obtained his Doctor degree in 1998 supervised by Tiejong Zuo, an academician of the Chinese Academy of Engineering. He joined the School of Materials Science and Engineering in Central South University (CSU) as an Associated Professor in 2000, and was promoted to a full professor in 2005. He has engaged in the development of rare-metal-based materials for

more than 20 years. Until now, he has published more than 80 papers and 15 patents, which are supported by National Science Foundations, 863 programs and military projects.